Cell Growth and Size Homeostasis in Proliferating Animal Cells

Amit Tzur,[1]* Ran Kafri,[1]* Valerie S. LeBleu,[2] Galit Lahav,[1] Marc W. Kirschner[1]†

A long-standing question in biology is whether there is an intrinsic mechanism for coordinating growth and the cell cycle in metazoan cells. We examined cell size distributions in populations of lymphoblasts and applied a mathematical analysis to calculate how growth rates vary with both cell size and the cell cycle. Our results show that growth rate is size-dependent throughout the cell cycle. After initial growth suppression, there is a rapid increase in growth rate during the G_1 phase, followed by a period of constant exponential growth. The probability of cell division varies independently with cell size and cell age. We conclude that proliferating mammalian cells have an intrinsic mechanism that maintains cell size.

A cell's growth may have a complex relationship to milestones in its life, specifically to its position in the cell cycle. In one model, growth rate is proportional to cell size at any time during the cell cycle (in whatever terms size is measured, e.g., volume, mass, or protein content); this constitutes exponential growth for an individual cell. Alternatively, the growth rate might be constant, producing a linear increase in size (*1*, *2*). These alternative models have important implications for how cell size is regulated. Specifically, the size of the daughter cells upon division is variable. If the larger daughter grows more rapidly than the smaller, as in the exponential model, cell size variation in the population would increase in each generation. Because this does not occur, we know that if growth is exponential—or, more generally, if it increases with cell size—some mechanism must limit size variation in cells (*3*–*5*).

In budding yeast, there is evidence both for a size-dependent growth rate (*6*) and for a process that coordinates growth with division in a way that potentially limits size variation (*1*, *7*–*9*). Whether there are similar growth controls in bacteria remains controversial (*10*–*12*). In metazoan cells, it is unclear whether such regulation exists at all. Because somatic cells do not grow as isolated cells, their size regulation might simply be the result of separate growth and mitogenic signals from the environment. Studies on primary Schwann cells suggested such a model; they provided evidence for a constant rate of growth independent of cell size (*13*–*15*). Yet these conclusions are also controversial (*16*, *17*), and other measurements of growth in mammalian cells have suggested that growth rate is proportional to size (*18*), implying a cell-sizing mechanism (*19*).

Attempts to measure growth during the cell cycle from time-series measurements confront major challenges. To obtain this information requires accuracy that is currently unattainable (*2*). Distinguishing between exponential and linear growth would need a resolution of <6% in volume (*20*). Even careful interferometric measurements in the classic experiments by Zetterberg and Killander

[1]Department of Systems Biology, Harvard Medical School, Boston, MA 02115, USA. [2]Division of Matrix Biology, Beth Israel Deaconess Medical Center and Harvard Medical School, Boston, MA 02215, USA.

*These authors contributed equally to this work.
†To whom correspondence should be addressed. E-mail: marc@hms.harvard.edu

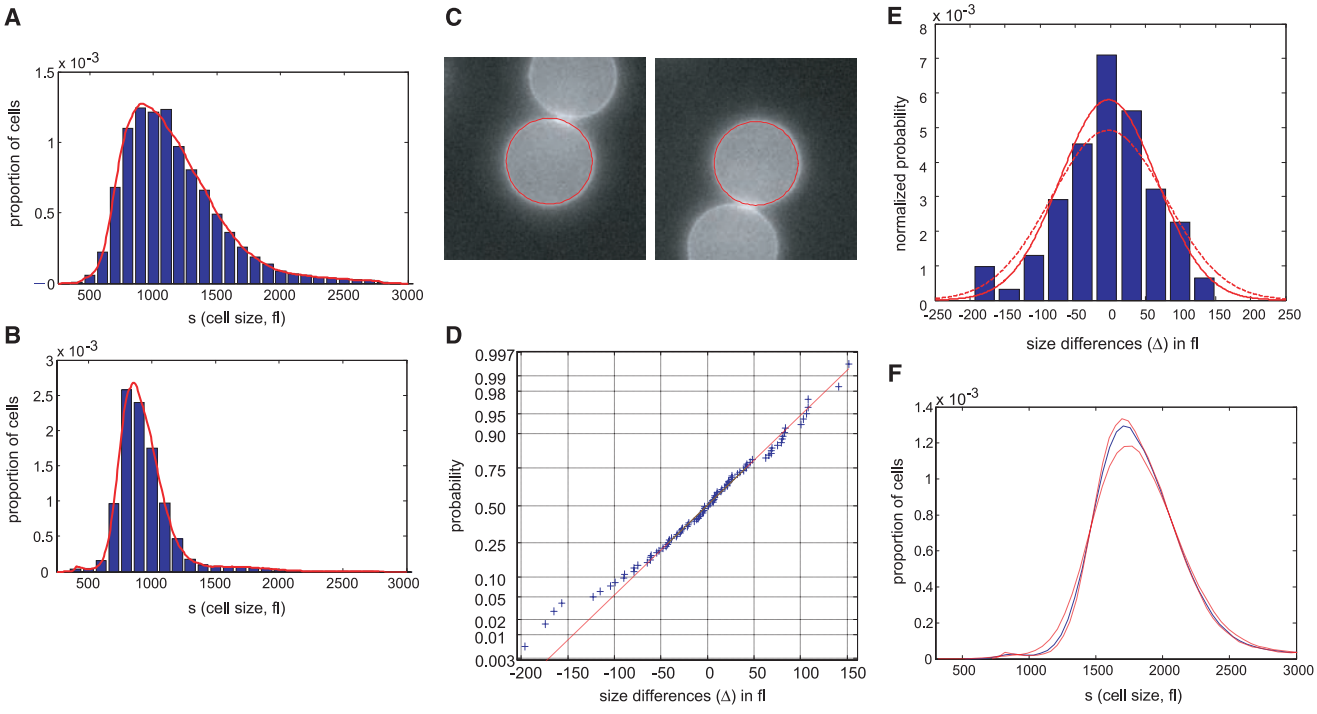

Fig. 1. Extracting parameters for calculating the size dependency of cell growth rate. (**A** and **B**) Size distribution of asynchronous steady-state populations (A) and newborn populations (B), shown by histograms (blue) and kernel density estimates (red). (**C**) L1210 cells, membrane-labeled with green fluorescent protein, were imaged while exiting mitosis. Each cell was fitted in a circle at maximum diameter. See (*20*) for details and error. (**D**) A quantile normal probability plot showing the normality of the daughter cell volume differences, Δ. (**E**) Distribution of size differences between daughter cells. A single parameter for the variance, σ^2, of the Gaussian estimate (solid red line) for the distribution, $\delta(\Delta)$. Also shown is the distribution corresponding to the upper confidence interval of the Gaussian estimate (dashed red line). (**F**) Mitotic size distribution calculated by convolving newborn size distribution with $\delta(\Delta)$. Confidence intervals of the $\delta(\Delta)$ distribution were used to generate the confidence of the mitotic size distribution (shown in red). See (*20*) for details.

failed to reach clear conclusions regarding the kinetics of cell growth (*21*, *22*).

Attempts to improve statistical accuracy by measuring large populations of cells foundered on the need to synchronize cells without affecting growth. Cell cycle inhibitors induce synchrony by blocking the nuclear cycle, but their effects on growth are unclear. Other procedures such as trypsinization, elutriation, and mitotic shake-off can also perturb the population in ways that are difficult to evaluate (*23*). In the 1960s, elegant mathematical approaches for extracting the rate of cell growth versus cell size were developed (*12*, *24*). These depend on isolating pure populations of both newborn and dividing cells, which has been difficult to achieve. Moreover, even with high-quality data, the analysis is ambiguous and incorrect (see below). We have now overcome these difficulties by combining a gentle cell synchronization technique (*25*) with mathematical analysis to determine accurately the growth function for lymphoblastoid leukemia cells.

Measuring the size dependency of growth in asynchronous populations. To calculate the dependence of growth rate on size, we applied a method that analyzes an asynchronous population at steady state, proposed by Collins and Richmond in 1962 (*12*). Specifically, at steady state, the number of cells smaller than size s increases only when cells larger than s divide and decreases only when cells smaller than s grow in size. Because the proportion of cells of any given size does not change with time, these two numbers must be equal (fig. S1).

Despite its mathematical simplicity, the Collins-Richmond method has been difficult to implement. In addition to the readily obtainable asynchronous size distribution, the method requires the size distribution of both the newborn subpopulation and the distribution of cells just before they divide, both of which are difficult to obtain. Under assumptions of unknown validity, the method has been used to suggest an exponential cell growth rate for bacteria (*12*) and for mammalian cells (*18*).

We can now obtain these distributions without unproven assumptions. To obtain the subpopulation of newborns, we grew mouse lymphoblasts (L1210) on a coated nitrocellulose membrane constantly bathed in a closed system (*25*). As these cells divide, one of the two daughters detaches from the membrane and the newborn cells are gently eluted. The remaining daughters can grow and divide, continually providing newborn cells. Two of the three needed size distributions are thus readily measured by Coulter Counter (Beckman Coulter Inc.): those for the unsynchronized populations (Fig. 1A) and newborn populations (Fig. 1B).

It is very difficult to isolate a uniform population of cells just before they divide. Instead, we calculate the mitotic (predivision) size distribution by combining the size distribution of newborns (Fig. 1B) with an experimentally determined size correlation between two daughter cells (Fig. 1, C to E). Specifically, the mitotic size distribution $f_m(s)$ (Fig. 1F) is calculated from the convolution $f_m(s) = (f_0 * \delta)(s)$, where $\delta(\Delta)$ is the distribution of the difference, Δ, in size between daughter cells emerging from mitosis (subtraction directionality is random), and f_0 is the size distribution of newborns. This calculation is valid only to the extent that Δ is independent of cell size, which we confirmed experimentally (*20*) (fig. S9). Volume differences between daughter cells closely follow a Gaussian distribution (σ = 66.8 ± 10 fl) and correspond to 7% of mean newborn volume. Comparing this value with the size variation of unrelated newborns (20.4%) demonstrates the remarkable accuracy of cytokinesis.

We thus have the data needed for the Collins-Richmond method without unproven assumptions. Equation 1 expresses the cell growth rate υ as a function of cell size s from three measurements: (i) the asynchronous size probability distribution, $f_a(s)$ [or $F_a(s)$ in its cumulative form]; (ii) the newborn cumulative size probability distribution, $F_0(s)$; and (iii) the distribution of differences between newborns, $\delta(\Delta)$:

$$\upsilon(s) = 2\alpha\frac{F_0(s)}{f_a(s)} - \alpha\frac{(F_0 * \delta)(s)}{f_a(s)} - \alpha\frac{F_a(s)}{f_a(s)} \quad (1)$$

where α is the fraction of dividing cells per unit time. The three terms on the right side of Eq. 1 represent the fact that the actual increase of cell number in a steady-state population (the rightmost or "population increase" term) must be balanced by cell growth rate (υ) on one hand and by division rate (i.e., the "newborns" and "mitotics" terms) on the other hand (fig. S1).

Applying Eq. 1 to our data sets shows how growth rate varies with cell size in the asynchronous population. Plots for L1210 mouse lymphoblasts (Fig. 2A) and MOLT4 human lymphoblasts (fig. S2) show similar relationships of growth rate and size. In both cell lines, larger cells are observed to have higher growth rates throughout

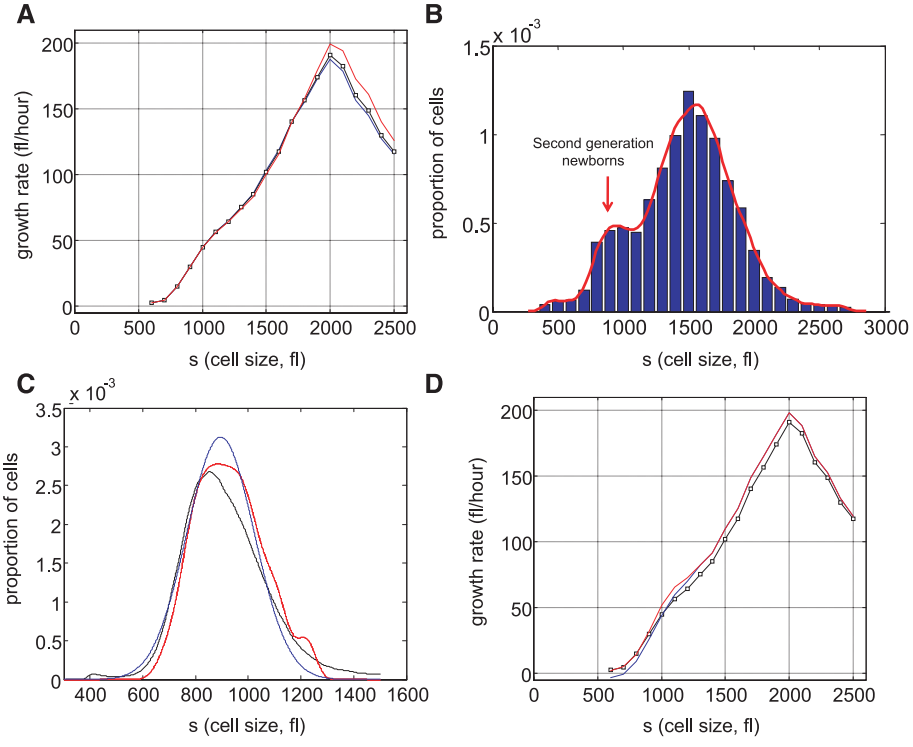

Fig. 2. Growth rate as a function of cell size. (**A**) Mean growth rate as a function of cell size for L1210 cells. Curve (black) was calculated from the Coulter Counter measurements of asynchronous size distribution (10^6 cells) and the size distribution of newborns (10^5 cells) together with the daughter cell correlation (see Fig. 1) using the Collins-Richmond method. Also shown are the curves based on the assumption of symmetric division (blue) and on a variance for daughter cell differences that is 2 times the measured value (red). Because of the large numbers of cells in the data sets, errors in growth rate obtained from this calculation are <1 fl/hour (*20*). (**B**) Bimodal size distribution of synchronous L1210 population at time t = 9 hours. The left mode represents second-generation newborns generated completely in suspension. (**C**) The similarity in the size distribution of the newborns freshly eluted from membrane versus the size distribution of newborns generated in suspension. The black curve corresponds to the size distribution of eluted newborns. We calculate the size distribution of the second-generation newborns (blue curve). The two size modes at t = 9 hours were separated using a Gaussian extrapolation. The red curve is an alternative extrapolation of the same distribution obtained by a method used later in the study to calculate the probabilities of cell division (see text). (**D**) The Collins-Richmond growth plot (black curve) was recalculated using second-generation newborns. Red and blue curves represent the different methods of extrapolating newborns.

most of the cell size range. However, beyond a critical size (cell volume = 2000 fl for L1210, 2500 fl for MOLT4), the trend is reversed and growth rates decline with increased size (Fig. 2A and fig. S2). Note that 65% of the L1210 population would have divided before reaching this size.

Although release of the unattached daughter cell would appear to be gentle and unperturbing, there is still concern that the daughter cell size distribution could be affected by the membrane. To test for this, we examined the size distribution of newborns produced completely in suspension, at the start of the second cell cycle (Fig. 2B). As shown in Fig. 2C, this estimated newborn distribution is very similar to that of the newborns obtained directly by elution, and, when integrated into the Collins-Richmond equation, the plot is nearly identical to that calculated from the eluted newborns (Fig. 2D).

Although growth rate appears to depend on size, growth rate heterogeneity in the population for each cell size can weaken this conclusion (*20*). Thus, even with a complete data set such as the one we have obtained, the Collins-Richmond method is inadequate to portray the growth of an individual cell over time. Resolution requires additional information that we obtain from an analysis of growth as a function of time.

Time dependency of growth. The synchrony of newborns eluted from the membrane allowed us to follow the change in the distribution of cell size with time (Fig. 3A). Specifically, we compared pairs of size distributions, f_n and f_{n+1}, sampled from the synchronized population at 1-hour intervals, $\Delta t = t_{n+1} - t_n = 1$ hour. Within such short time intervals, the growth of any single cell i can be accurately estimated by a simple linear function, $s^i(t) = s_0^i + \beta_n^i(t - t_n)$, regardless of the underlying complexity of the "real" growth function (*20*). Here, β_n^i and s_n^i are the growth constant and size of cell i in time interval n, respectively [i.e., time interval (t_n, t_{n+1})]. Cell-to-cell variation in growth rates is captured by the distribution of β_n^i values in each of the time intervals. Our aim is to calculate the average rate β_n at which cells grow in each time interval, as well as to provide an estimate for the cell-to-cell variation. We use β_n to denote the average of all β_n^i values in time interval n:

$$\beta_n = \frac{1}{N_t}\sum_{i=1}^{N_t}\beta_n^i \qquad (2)$$

Implementation of our method requires an assumption about the initial conditions of the time course. Specifically, we must specify how growth rates, $\{\beta_0^1, \beta_0^2, \ldots, \beta_0^i\}$, are to be paired with the measured sizes, $\{s_0^1, s_0^2, \ldots, s_0^i\}$, in the newborn population. The simplest possibility is that for newborn subpopulations, growth rate and size are independent. To test this assumption, we repeated the calculation with a different assumption: that growth rates are proportional to, rather than independent of, the cells' birth size. This latter simplification uses exponential, $s^i(t) = s_0^i \exp[k_n^i(t - t_n)]$, rather than linear functions to estimate growth in the separate time intervals; here, k_n^i is the exponential growth constant of cell i at time interval n.

Using the linear estimates, $s^i(t) = s_0^i + \beta_n^i(t - t_n)$, the growth rate υ of any single newborn cell is equal to its growth constant, β_0^i. By contrast, using the exponential functions, the growth rate of a newborn cell is given by $\upsilon = k_0^i s_0^i$. With the exponential estimates, it is k_n^i, rather than the actual growth rate, that is independent of cell size in the newborn population. As shown in Fig. 3, B and E, our method yields the same result regardless of whether linear or exponential estimates were used. This shows the power of our data to produce a single conclusion regardless of the specifics of the simplifying assumptions. Note that the assumption of growth constants (β or k) that are independent of cell size is invoked only for newborns; at the later time points, cells

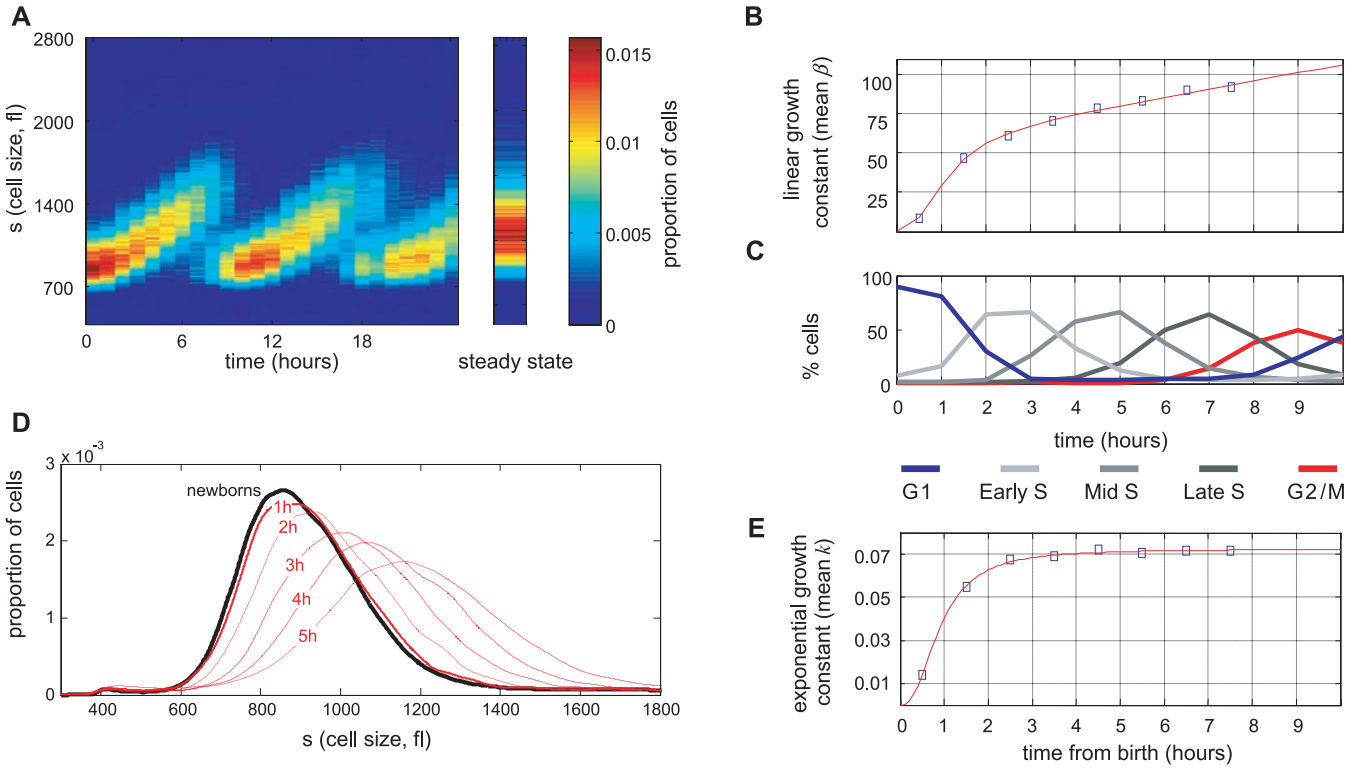

Fig. 3. Growth rate as a function of cell cycle. (**A**) Newborn L1210 cells were incubated at 37°C. Aliquots of cells were taken every hour from 0 to 24 hours to measure the size distribution of the synchronous population as it progressed through 2.5 cycles. Proportions of cells at any given size are visualized by color (see color bar at far right). Also shown is the time-invariant steady-state distribution of the asynchronous population. (**B**) Mean linear growth constants β_n (fl/hour) for each of the time intervals as calculated from Eqs. 3 to 6. (**C**) Distribution of cell cycle stages. (**D**) Growth repression visualized from raw size distribution measurements. Size distributions of the synchronized L1210 population are shown for early times in the cell cycle just after release from the membrane. The size distribution of newborns (black curve) is compared with distributions from t = 1 hour (heavy red curve) and t = 2 to 5 hours (lighter red curves). There is very little change from t = 0 to t = 1 hour, indicative of the growth repression during the first hour. The larger shifts in the size distribution for later times indicate faster growth later in the cell cycle. (**E**) Mean exponential growth constants k_n (hour^{-1}) for each of the time intervals as calculated in (*20*).

with larger growth constants will have accumulated more mass and volume than cells with smaller growth constants and will inevitably be larger.

With the linear estimates, we calculate growth rates by representing the size of a cell at time n, s_n^i, as a sum of its newborn size, s_0^i, together with a size difference c_n^i; that is, $s_n^i = s_0^i + c_n^i$ (every size is compared to the initial newborn size). With this notation, relying on the simplifying assumption described above, we search for the set of values $\{c_n^1, c_n^2, c_n^3, \ldots, c_n^N\}$ that, when randomly paired with and added to the measured sizes from the newborn population, would produce a set of values $\{x^1, x^2, \ldots, x^N\}$ (i.e., $x^i = c_n^j + s_n^i$) that have the same probability distribution as the measured cell sizes $\{s_n^1, s_n^2, \ldots, s_n^N\}$ from time interval n.

In more conventional statistical language, we describe the probability distribution of c_n^i with $\varphi_n(c)$ and use c_n to denote the mean c value at time $t = n$. We express the measured distribution f_n, from time n, as a convolution of the measured distribution of newborn sizes f_0 with $\varphi_n(c)$, $f_{n(\text{measured})} = f_{0(\text{measured})} * \varphi_n$ (Eq. 3), and solve for $\varphi_n(c)$ by numerical deconvolution. From $\varphi_n(c)$ we use Eq. 4 to calculate the mean value c_n for each time point; we then use Eqs. 5 and 6 to relate the calculated c_n values to the mean growth rates β_n:

$$f_n(s) = \int_{c=0}^{\infty} f_0(s-c)\varphi_n(c)dc \qquad (3)$$

$$c_n = \int c\varphi_n(c)dc = \langle c_j^i \rangle \qquad (4)$$

$$\beta_n = c_n - \sum_{j=0}^{n-1} \beta_j \Delta t \qquad (5)$$

Because $\Delta t = 1$,

$$\beta_n = c_n - \sum_{j=0}^{n-1} \beta_j \qquad (6)$$

In Eq. 3, f_0 and f_n are experimentally measured distributions; thus, by numerical deconvolution, we solve Eq. 3 for the probability distribution $\varphi_n(c)$. We can then recursively calculate mean growth values for each time interval by plugging the calculated c_n into Eq. 6, where c_n is simply the average of the probability distribution $\varphi_n(c)$. After independently calculating the growth estimates for each of the 1-hour segments throughout the cell cycle, the true functional form of the growth function was reconstituted by linking the successive 1-hour segments (*20*). Thus, Eqs. 3 to 6, and their more general formulation in (*20*), provide a means of calculating the average growth rate between any two time points if the size distributions at these time points and the size distribution of newborns are known.

Figure 3B shows the results of applying Eqs. 3 to 6 to the synchronized population of L1210 mouse lymphoblasts. It reveals that the average rate of cell growth β_n, calculated by the linear segmental estimates, increases rapidly at the early stages of cell cycle and is then followed by a slower linear increase until cell division starts (see Fig. 3C, which relates Fig. 3B to cell cycle stages). The suppression of growth in G_1 (Fig. 3B) can be directly observed from the experimental size distribution curves for the synchronous L1210 populations (Fig. 3D).

Using the exponential growth model (*20*), the post-G_1 period is seen to be described precisely with an exponential growth rate constant of $k = 0.07$ hour^{-1} or a growth rate of $0.07s$ (Fig. 3E). Combined, Fig. 3B and Fig. 3E provide a description of cell growth. In Fig. 3B, growth is expressed with a linear growth constant, β (fl/hour), which increases with time in the post-G_1 period, whereas in Fig. 3E, growth is expressed with an exponential constant, k (hour^{-1}), which does not change during that same period.

From the resulting distributions $\varphi_n(c)$, we calculate that the total variation in growth rates in the population is CV = 49%. This variation is composed from the size variation and a variation in exponential constants, which were independently calculated as 32% and 18%.

This analysis allows us to interpret the Collins-Richmond plot (Fig. 2A) in terms of growth rate changes during the cell cycle. In Fig. 3B, the growth rate β increases from 10 fl/hour during G_1 to 90 fl/hour as cells progress toward division. From Fig. 3 we now realize that this factor of 9 increase is largely localized to the early G_1 phase—an age dependency that is lost in the Collins-Richmond representation because of a poor correlation between cell size and age (*20*) (figs. S3 and S4).

Dependence of cell division on time and size. These results require some size control mechanism to limit the dispersion in cell sizes. To test for the possibility that there is a size gate that shortens the cell cycle for large cells, we examined the interval in which most cells divide (9 to 12 hours after birth; Fig. 3A). By using the growth constants that we determined in Fig. 3E and comparing the measured size distributions from two consecutive times, we can calculate the frequency of cell divisions in this population as a function of cell cycle time (Fig. 4). To take one example, consider the number of cells that, at 8 hours after birth, are contained in the size interval (s_1, s_2) (cells larger than s_1 and smaller than s_2). Given a value of $k = 0.07$ hour^{-1} (Fig. 3E), at 9 hours after birth, these same cells will be contained by the interval $\{s_1 \exp(0.07), s_2 \exp(0.07)\}$. Any deviation from this equivalence can only occur by division. To avoid confusion with newborn cells, we calculate the division frequencies using cells of size 1500 fl or larger, where the proportion of newborns is negligible (Fig. 1B).

We found that for cells of the same age, the likelihood of division increases with cell size (Fig. 4A). Also, for cells of the same size, older cells have a greater chance to divide than do younger cells (Fig. 4B). Thus, the likelihood of cell division, ψ, is governed by both cell age τ and cell size s. More explicitly, the probability for cell division follows a differential form,

$$d\psi = \left(\frac{\partial \psi}{\partial \tau}\right)_s d\tau + \left(\frac{\partial \psi}{\partial s}\right)_\tau ds \qquad (7)$$

where the dependency of cell division on cell size and age is captured by the partial derivatives $[\partial\psi(\tau,s)/\partial\tau]_s$, where size is held constant, and $[\partial\psi(\tau,s)/\partial s]_\tau$, where age is held constant.

Our current measurements lack the accuracy to obtain these partial derivatives to high precision. Nonetheless, by relying on linear fit estimates, we can obtain approximations for their magnitudes: roughly $(\partial\psi/\partial s)_\tau = 0.0002 \pm 0.0001$ fl^{-1} at 9 hours after birth and 0.0004 ± 0.0001 fl^{-1} at 12 hours after birth, and $(\partial\psi/\partial\tau)_s = 0.008 \pm 0.03$ hour^{-1} for cells of volume 1500 fl and 0.1 ± 0.02 hour^{-1} for cells of volume 2400 fl.

Discussion. The size of a cell reflects the relationship between its growth rate and division

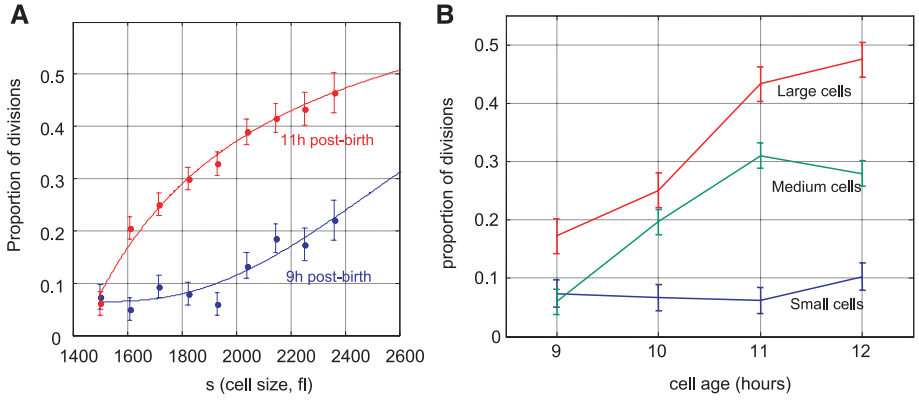

Fig. 4. Frequency of cell division as a function of cell size and age. (**A**) For cells of the same age, the probability of division increases with cell size. Proportions of cells that have divided at any specified size are shown for cells at 9 hours after birth (blue curve) and 11 hours after birth (red curve). At 11 hours after birth, about 20% of all cells of size 1600 fl divide. Size distributions were calculated on the basis of a Gaussian kernel. (**B**) For cells of the same size, the probability of division increases with cell age. Division frequencies as a function of age (each time point represents a 1-hour interval starting at the indicated times) are shown for cells with size ranging from 1500 to 1850 fl (blue curve), from 1850 to 2200 fl (green curve), and from 2250 to 2500 fl (red curve).

frequency. It has been difficult to study in metazoan cells, due primarily to the lack of sufficiently accurate, sensitive, and reliable means of measurement. We have addressed these deficiencies with mathematical and experimental methods that allow us to describe the growth of individual cells during the cell cycle from measurements made on very large samples. Although we are measuring the cell volume, other studies have shown that the buoyant density of cells remains constant through the cell cycle, implying that volume can be used as a surrogate for mass (*26*, *27*).

For mouse lymphoblastoid cells, we find an accelerative growth phase in G_1 (where an exponential rate constant is itself time-dependent), followed by a period of stable exponential growth during the rest of the cell cycle. Thus, at least for this cell type, our results settle a long-standing controversy of whether mammalian cell growth can be described by linear or exponential kinetics. The true growth function across the cell cycle is neither a simple exponential nor a linear function, and it is size-dependent. Therefore, mammalian cells must possess a cell-autonomous intrinsic size regulator that couples cell growth to the cell cycle.

In fission yeast, entry into mitosis has been shown to be size-dependent, whereas in budding yeast, division is set by a "timer" activated at the start point (*1*). For lymphoblasts, we find that growth and division are independently determined by cell size and age. The correlation between size and division in mammalian cells thus cannot be a simple consequence of either size-independent processes that govern cell cycle duration or a size gate that feeds back on the timing of the cell cycle.

Our data contrast with the data from Raff and colleagues (*13*) on adherent Schwann cell cultures, where a linear dependence of growth on size was suggested. This might reflect differences between adherent and suspension cell populations, their use of drugs to induce synchrony, or the difference in the type of cell studied. In addition, their Schwann cells were allowed to grow without division, reaching an extreme size (*13*). We found that very large cells above a critical cell size (2000 fl for L1210 cells—a size never attained by most of the growing cells in the culture) displayed growth behavior different from the cells that divided at smaller size. In this regime, growth is no longer proportional to size and could appear linear.

Although much has been learned about growth and cell division in mammalian cells, the circuits that coordinate these processes have not yet been investigated. The analytical tools presented here should facilitate the study of the biochemical circuitry responsible for setting the size and maintaining the limits of cell size variation, despite the potentially disruptive consequences of size dependence of growth. Given the very large size differences of different somatic cell types, the processes governing cell size would be expected to be deeply enmeshed in developmental mechanisms and subject to physiological constraints.

References and Notes

1. P. Jorgensen, M. Tyers, *Curr. Biol.* **14**, R1014 (2004).
2. J. M. Mitchison, *Int. Rev. Cytol.* **226**, 165 (2003).
3. E. Trucco, *Bull. Math. Biophys.* **32**, 459 (1970).
4. E. Trucco, G. I. Bell, *Bull. Math. Biophys.* **32**, 475 (1970).
5. J. J. Tyson, K. B. Hannsgen, *J. Math. Biol.* **22**, 61 (1985).
6. S. G. Elliott, C. S. McLaughlin, *Proc. Natl. Acad. Sci. U.S.A.* **75**, 4384 (1978).
7. P. Jorgensen, J. L. Nishikawa, B.-J. Breitkreutz, M. Tyers, *Science* **297**, 395 (2002); published online 27 June 2002 (10.1126/science.1070850).
8. D. R. Kellogg, *J. Cell Sci.* **116**, 4883 (2003).
9. S. Di Talia, J. M. Skotheim, J. M. Bean, E. D. Siggia, F. R. Cross, *Nature* **448**, 947 (2007).
10. H. E. Kubitschek, *Biophys. J.* **8**, 1401 (1968).
11. H. E. Kubitschek, *J. Bacteriol.* **168**, 613 (1986).
12. J. F. Collins, M. H. Richmond, *J. Gen. Microbiol.* **28**, 15 (1962).
13. I. Conlon, M. Raff, *J. Biol.* **2**, 7 (2003).
14. I. J. Conlon, G. A. Dunn, A. W. Mudge, M. C. Raff, *Nat. Cell Biol.* **3**, 918 (2001).
15. P. Echave, I. J. Conlon, A. C. Lloyd, *Cell Cycle* **6**, 218 (2007).
16. S. Cooper, *BMC Cell Biol.* **5**, 35 (2004).
17. A. Sveiczer, B. Novak, J. M. Mitchison, *Theor. Biol. Med. Model.* **1**, 12 (2004).
18. E. C. Anderson, G. I. Bell, D. F. Petersen, R. A. Tobey, *Biophys. J.* **9**, 246 (1969).
19. H. Dolznig, F. Grebien, T. Sauer, H. Beug, E. W. Mullner, *Nat. Cell Biol.* **6**, 899 (2004).
20. See supporting material on *Science* Online.
21. D. Killander, A. Zetterberg, *Exp. Cell Res.* **38**, 272 (1965).
22. A. Zetterberg, D. Killander, *Exp. Cell Res.* **39**, 22 (1965).
23. S. Cooper, *Cell. Mol. Life Sci.* **60**, 1099 (2003).
24. G. I. Bell, E. C. Anderson, *Biophys. J.* **7**, 329 (1967).
25. V. S. LeBleu, M. Thornton, R. G. Gonda, C. E. Helmstetter, *Cytotechnology* **51**, 149 (2006).
26. E. C. Anderson, D. F. Petersen, R. A. Tobey, *Biophys. J.* **10**, 630 (1970).
27. M. R. Loken, H. E. Kubitschek, *J. Cell. Physiol.* **118**, 22 (1984).

28. We thank C. Helmstetter and J. Horn for sharing plans and construction of the newborn cell device; S. Cooper for suggesting we consider that device for cell cycle studies; J. Levy for discussions and for advice with the mathematical analyses; J. Waters and the Nikon Imaging Centre for help with the microscopy; C. Mock for cell sorting; G. Charras and T. Balla for reagents; and S. Tal, J. Toettcher, P. Bordalo, R. Milo, T. Mitchison, P. Jorgensen, G. Charras, E. Zlotorynski, S. Dumont, N. Shoresh, and M. Springer for advice and critical reading. Supported by NIH grant GM083303 (G.L.), a Human Frontier Science Program fellowship (R.K.), and NIH grant GM026875.

Supporting Online Material

www.sciencemag.org/cgi/content/full/325/5937/167/DC1
Materials and Methods
Figs. S1 to S11
Tables S1 and S2
References

31 March 2009; accepted 15 May 2009
10.1126/science.1174294

REPORTS

Penumbral Structure and Outflows in Simulated Sunspots

M. Rempel,[1]* M. Schüssler,[2] R. H. Cameron,[2] M. Knölker[1]

Sunspots are concentrations of magnetic field on the visible solar surface that strongly affect the convective energy transport in their interior and surroundings. The filamentary outer regions (penumbrae) of sunspots show systematic radial outward flows along channels of nearly horizontal magnetic field. These flows were discovered 100 years ago and are present in all fully developed sunspots. By using a comprehensive numerical simulation of a sunspot pair, we show that penumbral structures with such outflows form when the average magnetic field inclination to the vertical exceeds about 45 degrees. The systematic outflows are a component of the convective flows that provide the upward energy transport and result from anisotropy introduced by the presence of the inclined magnetic field.

Sunspots are dark patches on the visible solar surface that harbor strong magnetic fields up to 4000 G (*1*, *2*). Their central region, the umbra, is the darkest part, with a brightness of about 20% of the ambient value and a largely vertically oriented magnetic field; the brighter, filamentary penumbra shows a more inclined field and a nearly horizontal plasma outflow of several $km \cdot s^{-1}$, the Evershed flow, which was named after its discoverer (*3*). Although a number of simplified (and partly conflicting) models have been suggested to explain the structure and outflows of penumbrae (*4*), a comprehensive theoretical understanding of the basic mechanisms does not exist.

Here, we present ab initio numerical simulations of complete sunspots embedded in a realistic solar convection zone and atmosphere, including all relevant physical processes: compressible magnetohydrodynamics, partial ionization, and radiative energy transport. Previous attempts to simulate penumbral structure in small slablike sections of sunspots (*5*, *6*) resulted in rather narrow penumbral regions. The generally used periodic boundary conditions at the sides of

[1]High Altitude Observatory, National Center for Atmospheric Research (NCAR), Post Office Box 3000, Boulder, CO 80307, USA. [2]Max-Planck-Institut für Sonnensystemforschung, Max-Planck-Straße 2, 37191 Katlenburg-Lindau, Germany.

*To whom correspondence should be addressed. E-mail: rempel@hao.ucar.edu